International Journal of Nanomedicine

Dovepress

open access to scientific and medical research

Open Access Full Text Article

ORIGINAL RESEARCH

Hydrogels Containing Chitosan-Modified Gold Nanoparticles Show Significant Efficacy in Healing Diabetic Wounds Infected with Antibiotic-Resistant Bacteria

Hongqi Meng[1], Ying Zhao[1], Hang Cai[2], Di You[3], Ying Wang[4], Siyu Wu[1], Yixin Wang[5], Wenlai Guo[1], Wenrui Qu[1,6]

[1]Department of Hand Surgery, The Second Hospital of Jilin University, Changchun, 130041, People's Republic of China; [2]Department of Pharmacy, The Second Hospital of Jilin University, Changchun, 130041, People's Republic of China; [3]Department of Anesthesiology, China-Japan Union Hospital of Jilin University, Changchun, 130031, People's Republic of China; [4]Institute of Neural Tissue Engineering, Mudanjiang College of Medicine, Mudanjiang, 157011, People's Republic of China; [5]Department of Plastic Surgery, First Hospital of Jilin University, Changchun, 130021, People's Republic of China; [6]Joint International Research Laboratory of Ageing Active Strategy and Bionic Health in Northeast Asia of Ministry of Education, Jilin University, Changchun, 130041, People's Republic of China

Correspondence: Wenlai Guo, Email guowl19@jlu.edu.cn

Purpose: Persistent Infections and inflammation are associated with impaired wound healing in diabetic patients. There is a pressing demand for innovative antimicrobial strategies to address infections arising from antibiotic-resistant bacteria. Polymer-modified gold nanoparticles (AuNPs) show broad-spectrum antibacterial properties and significant biocompatibility. This study investigated the antibacterial and wound healing efficacy of hydrogel dressings conjugated with chitosan-AuNPs in diabetic model rats.

Methods: Chitosan (CS)-functionalized gold nanoparticles (CS-AuNPs) were incorporated into hydrogel dressings (Gel/CS-AuNPs), which were formulated through the chemical cross-linking of gelatin with sodium alginate (SA). The basic characteristics of Gel/CS-AuNPs were analyzed by TEM, SEM, XRD, and UV-visible spectra. Rheological, swelling, degradation, and adhesive properties of Gel/CS-AuNPs were also determined. In vitro anti-bactericidal effects of the Gel/CS-AuNPs were analyzed with *E. coli, S. aureus*, and *MRSA*. In vitro biocompatibility of the Gel/CS-AuNPs was evaluated using NIH3T3 cells. The in vivo antibacterial and wound healing efficacy of the Gel/CS-AuNPs was analyzed in the diabetic wound model rats. Histological and immunofluorescence staining were performed to determine the status of angiogenesis, epithelization, inflammation response, and collagen deposition.

Results: Gel/CS-AuNPs demonstrated significant high biodegradability, water absorption bactericidal, and biocompatibility, and slight adhesiveness. Gel/CS-AuNPs exhibited pronounced antibacterial efficacy against gram-negative, gram-positive, and *MRSA* in a CS-AuNPs-dose-dependent manner. In the diabetic wound model rats, Gel/CS-AuNPs effectively killed *MRSA*, reduced inflammation, and promoted angiogenesis and collagen deposition and remodeling at the wound site. As a result, Gel/CS-AuNPs expedited the recovery process for infected diabetic wounds. Among the hydrogels with different CS-AuNPs concentrations, Gel/CS-Au_{25} with 25% CS-AuNPs showed the best bactericidal and wound healing performance.

Conclusion: Gel/CS-AuNPs significantly improve the healing of *MRSA*-infected diabetic wounds in the rat model. Therefore, Gel/CS-AuNPs show great promise for the treatment of diabetic infection wound healing.

Keywords: *MRSA*, infection, diabetic wounds, hydrogels, CS-AuNPs, antimicrobial

Introduction

Diabetes affects approximately 463 million individuals globally, with nearly a quarter of this population experiencing persistent, non-healing wounds.[1–3] Diabetic wounds are highly susceptible to bacterial infections that can induce inflammation, which inhibits angiogenesis and wound healing, thereby aggravating the blood flow disorder.[4–6] Clinically, the long-term use of antibiotics to control infections in diabetics has resulted in the emergence of drug-

Received: 5 November 2023
Accepted: 5 February 2024
Published: 19 February 2024

Graphical Abstract

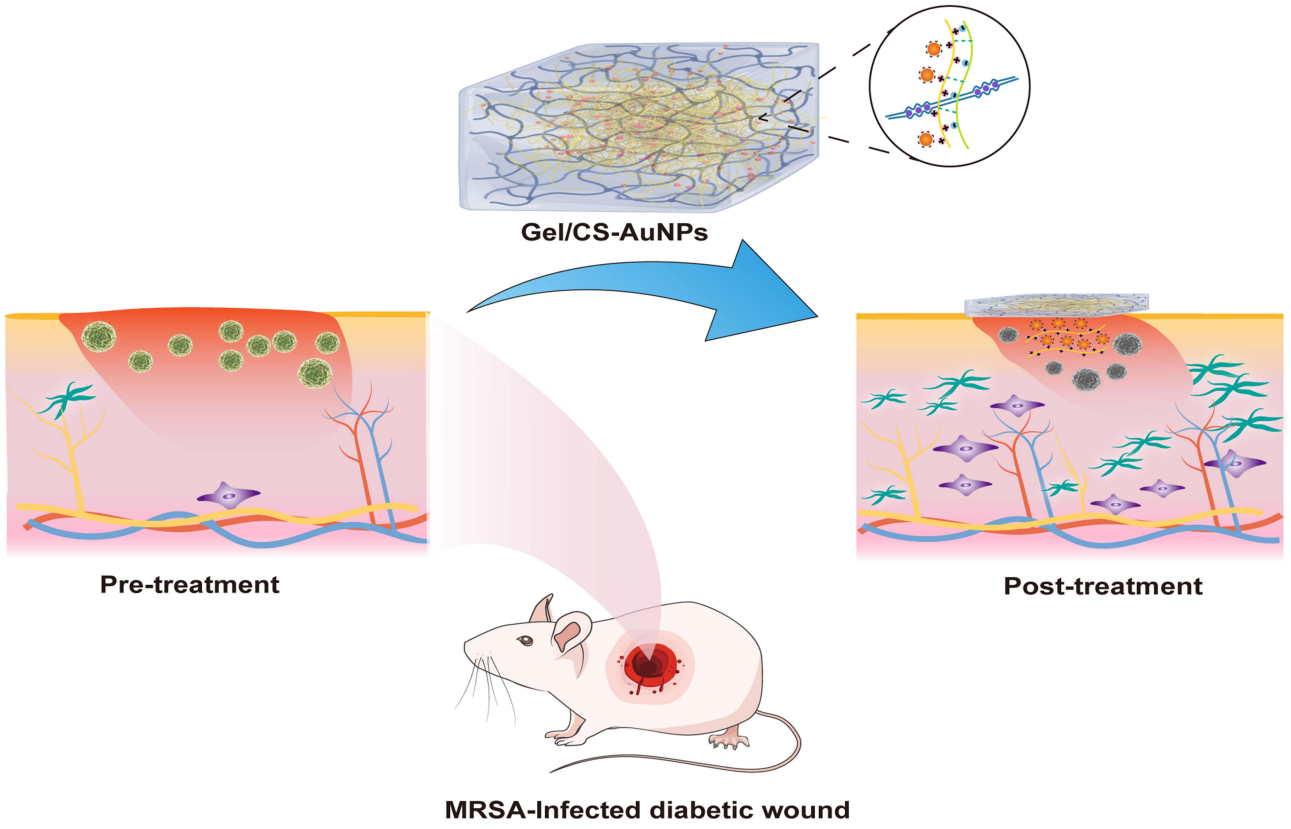

resistant bacterial strains.[4,7] Hence, there is a pressing demand for the innovation of novel, broad-spectrum, and low-toxic antimicrobial strategies that are effective in treating the infected wounds in diabetics.

Inorganic nanoparticles show excellent antibacterial properties and do not easily develop drug resistance.[7,8] AuNPs are amenable to surface functionalization and show high biocompatibility and stability.[9,10] Free AuNPs do not show antibacterial properties. However, light stimulation or ligand modification can enhance the antibacterial activities of the AuNPs.[11–13] The ligand-modified AuNPs show antibacterial activity by disrupting the integrity of the bacterial membranes through direct multivalent interactions.[12] AuNPs modified with ligands such as 4, 6-diamino-2-pyrimidine thiol (DAPT), polyhexamethylene biguanide (PHMB), and methimazole (MTM) show potent bactericidal effects.[12,14,15] However, DAPT, PHMB, MTM and AuNPs do not show significant antibacterial activity on their own. CS is a natural, positively charged cationic polymer. This unique cationic property enables CS to exhibit a broad spectrum of antimicrobial properties by associating with the negatively charged particles on the surface of the bacterial cells, however, its antibacterial ability is limited.[16–19] Therefore, in this study, AuNPs were modified with CS through electrostatic interactions to form CS-AuNPs so that the synergistic effects of the gold core and the surface ligands could further enhance the antibacterial effects.

Hydrogel demonstrate better adhesive properties than wound dressings with rubber, semi-permeable membrane, film, or foam, and does not easily fall off from the wound surface.[20] Hydrogel is also an ideal wound dressing, given its capacity to absorb and retain moisture. Therefore, hydrogels can absorb inflammatory exudates of the wound and maintain a moist environment.[5,21] In this study, we used gelatin and SA to generate a biodegradable hydrogel with good biocompatibility. Then, the CS-AuNPs were loaded onto hydrogels to form Gel/CS-AuNPs. Subsequently, we evaluated the efficacy of Gel/CS-AuNPs to heal wounds infected with antibiotic resistance in the diabetic model rats by analyzing the characteristics of wound healing, including the status of inflammation, wound epithelialization, angiogenesis, and collagen deposition.

Materials and Methods

Materials

Gelatin (gel strength 300, Type A) and chitosan [CS; low molecular weight, deacetylated chitin, Poly (D-glucosamine)] were purchased from Sigma-Aldrich Corporation (USA). Sodium alginate (SA, AR), glacial acetic acid (AR, 99.5%) and calcium chloride ($CaCl_2$) were obtained from Shanghai Aladdin Biochemical Technology Co. Ltd. (Shanghai, China). Tetrachloroauric acid tetrahydrate ($HAuCl_4.4H_2O$, 99.99%) and sodium citrate were purchased from China National Medical Corporation Ltd. (Beijing, P. R. China). The LIVE/DEAD BacLight Bacterial Viability Assay Kit was acquired from Molecular Probes (Eugene, OR, USA). Primary antibodies targeting interleukin-10 (IL-10), tumor necrosis factor-α (TNF-α), and cluster of differentiation 31 (CD31) were procured from BIOSS Biotechnology Co., Ltd. (Beijing, China). Mouse embryonic fibroblast cell line (NIH/3T3 cells) were purchased from Solarbio Co., Ltd (Beijing, China). *S. aureus* (ATCC 25923), *E. coli* (ATCC 25922), and *MRSA* (ATCC 43300) were purchased from Beijing Baocang Biotechnological Co., Ltd (Beijing, China). Male Sprague-Dawley rats, 6–8 weeks old and meeting SPF-grade standards, were sourced from Liaoning Changsheng Biotechnology Co., Ltd. (Liaoning, China).

Preparation of Hydrogel Dressings with CS/AuNPs

We mixed 2 mL of 1% $HAuCl_4.4H_2O$, 94.5 mL of ultrapure water, and 3.5 mL of 2% sodium citrate at 60°C using a magnetic stirrer and obtained a solution of 0.1 mg/mL AuNPs that was red colored. We dissolved 1.0 g of CS in 94.5 mL of 1% glacial acetic acid by continuous stirring at 60 °C until the solution was clear. Then, we added 2 mL of 1% $HAuCl_4.4H_2O$ solution and 3.5 mL of 2% sodium citrate to the mixture to obtain a solution of CS-AuNPs by continuous stirring at 60°C until the color of the solution turned red and remained stable. Gelatin and SA were added to the dispersion of CS-AuNPs at different concentrations. The mixture was stirred continuously for 12 h at 60°C. Then, the mixture was transferred into a mold and cross-linked for 2 minutes by adding 4mL solution of 5% $CaCl_2$. CS-AuNPs were prepared as hydrogel dressings containing 0% Gel (Gelatin/SA), 5% (Gel/CS-Au_5), 10% (Gel/CS-Au_{10}), 25% (Gel/CS-Au_{25}), and 50% (Gel/CS-Au_{50}).

Transmission Electron Microscopy (TEM)

The morphology and size distribution of AuNPs and CS-AuNPs were examined through TEM (JEM-2010 HT, JEOL, Japan), operating at 200 kV. TEM images were captured and subsequently analyzed using Image J software.

Estimation of the Zeta Potential, X-Ray Diffraction (XRD) and UV–Visible Spectroscopic Determination

The Malvern Zeta sizer Nano ZS system (Malvern Instruments Ltd., Worcestershire, UK) was used to assess the zeta potential of AuNPs and CS-AuNPs at 25 °C. The XRD patterns of AuNPs and CS-AuNPs were obtained with a Diano X-ray diffractometer and a Philips X-ray diffractometer at 45 kV, 4°/min, and a scanning range of 5° ~ 80°. The UV-visible absorption spectra of AuNPs and CS-AuNPs were measured at ambient temperature using a spectrophotometer (JENWAY 6305 Stone, UK) within the 300–800 nm wavelength range.

Fourier Transform Infrared Spectroscopy (FT-IR)

The Fourier coefficients of the infrared spectra were acquired using an FT-IR spectrophotometer (SHIMADZU, IRAFFINITY-1S, Japan) to assess the chemical structure and functional group of the materials at wavelengths ranging from 4000 to 500 cm^{-1}.[22]

Scanning Electron Microscopy (SEM) and Energy-Dispersive X-Ray Spectroscopy (EDS)

SEM (JSM-6700F, JEOL, Tokyo, Japan) was used to determine the morphology of different groups of hydrogels. Samples were prepared following the experimental methodology outlined by Guan et al.[5] Scanning electron micrographs were captured using an accelerating voltage set at 15 kV and a magnification of 50X. The SEM images were analyzed

using the Image J software to determine the pore size. Subsequently, Gel/CS-Au_{25} was scanned by SEM and EDS mapping was performed to determine element content and distribution.

Rheological Analysis of Hydrogels

The hydrogel's rheological characteristics were examined with a rheometer (TA DHR-3, USA).[23] The hydrogel samples were placed between 25 mm parallel plates with 1000 μm spacing. The hydrogels' energy storage modulus (G') and loss modulus (G") were assessed under oscillatory conditions, maintaining a constant 5% strain, and conducting measurements at 37°C over a range of 1 to 100 rad/s.

Estimation of Swelling Rate (SR) of Hydrogels

SR of the hydrogels was determined through the assessment of their wet weight change following incubation with phosphate-buffered saline (PBS). Specifically, the mass of the original damp hydrogel was recorded as M_0. Then, the hydrogel was incubated in PBS at 37°C. At minutes 30, 60, 90 and 120, the hydrogel was removed from the PBS and the mass was recorded as M_t. SR was calculated as $(M_t\text{-}M_0)/M_0 \times 100\%$. The measurements were repeated in triplicate samples. The periphery of the hydrogel was coated with silicone oil throughout the assay to prevent water loss.

Estimation of the Degradation Rate of the Hydrogels

The in vitro degradation rate was determined by analyzing the change in mass of lyophilized hydrogels over time. The same volume of lyophilized samples from each group of hydrogels were placed in PBS containing collagenase type II (0.6 μg/mL) and shaken at a constant rate of 100 revolutions per minute in an incubator maintained at 37°C. On days 1, 3, 5, and 7, the hydrogels were removed from the incubator, underwent three times cleaning process with distilled water to eliminate excess PBS, lyophilized, and weighed. The degradation rate (%) of the samples was determined using the formula: Degradation rate(%)$=M_t/M_0 \times 100\%$, where M_t represents the sample mass after immersion for a specified time "t", and M_0 denotes the initial mass of the sample before immersion in PBS.

Estimation of the Accumulated Release of CS-AuNPs from the Hydrogels

Four distinct hydrogel formulations, each with a consistent volume of 7 mL, were introduced into a centrifuge tube containing 21 mL of PBS. This assembly was then placed within a shaking chamber operating at a constant temperature of 37°C and a rotational speed of 150.0 rpm. At designated intervals (1, 2, 3, 4, and 5 days), 3 mL aliquots of the solution were withdrawn, and an equivalent volume of fresh PBS was replenished. Following adjustment to a constant volume of 10 mL, the prepared sample was subjected to injection. The Au content within the sample was quantified utilizing an inductively coupled plasma mass spectrometer (Agilent 5110) with the application of the external standard method.

$$Q(\%) = (C_i \times V + \sum_{i-1}^{n-1} C_{i-1} \times V_i)/m \times 100\%$$

In the context of this study, Q represents the cumulative release of AuNPs. C_i stands for the concentration of the liquid released during the i-th replacement sampling, while C_{i-1} represents the concentration from the preceding (i-1)-th replacement sampling. V_i denotes the displacement volume of the receiving solution, and V represents the total volume of the release medium, specifically set at 21 mL. The variable "n" corresponds to the number of times the receiving solution is replaced, and "m" signifies the total mass of AuNPs present in the hydrogels.

Estimation of Hydrogel Adhesive Properties

We performed macroscopic experiments to investigate the tissue adhesive properties of the hydrogels. The synthetic hydrogel was applied to the fingers and hand joints of the author. Subsequently, joint adhesion was documented while performing various angular movements.

In vitro Effects of Gel/CS-AuNPs on Cell Proliferation and Viability

The impact of Gel/CS-AuNPs on the growth and viability of NIH3T3 fibroblasts was assessed through the utilization of both the cell counting kit-8 (CCK-8) and live/dead cell labeling assays. For the CCK-8 assay, hydrogel extracts were prepared by co-culturing the hydrogels (Gel/CS-Au_5, Gel/CS-Au_{10}, Gel/CS-Au_{25}, and Gel/CS-Au_{50}) with Dulbecco's modified eagle medium (DMEM) at 37°C for five days. NIH3T3 cells were cultured with hydrogel extracts at 37°C. The cells were initially seeded in 96-well plates at an approximate density of 4×10^3 cells per well. On days 1, 3, and 5, the cells were incubated with the CCK-8 assay reagent for 2 h. Subsequently, a microplate reader measured the absorbance value at 450 nm. Cell viability was determined using the formula: Cell viability(%)= $OD_t/OD_c\times100\%$, where OD_t and OD_c represent the absorbance values of the treatment and control groups, respectively. In the live/dead cell staining procedure, NIH3T3 cells were seeded into 24-well plates at a concentration of 5×10^4 cells/mL per well and cultured for 24 h. Then, the cells were treated with different hydrogel solutions (Gel/CS-Au_5, Gel/CS-Au_{10}, Gel/CS-Au_{25} and Gel/CS-Au_{50}) for 24 h. The dead and live cells underwent staining with calcein AM and propidium iodide (PI) fluorescent dyes for 30 minutes. The live cells showed green fluorescence with calcein AM. The dead cells showed red fluorescence with PI. The stained cells were photographed under an inverted fluorescence microscope.

In vitro Antibacterial Effects of Gel/CS-AuNPs

The antibacterial effects of Gel/CS-AuNPs were evaluated using the inhibition zone and colony counting methods. *E. coli, S. aureus*, and *MRSA* cultures were sub-cultured in appropriate media. Bacteria suspensions at a concentration of 10^7 to 10^8 CFU/mL were uniformly coated on Luria-Bertani (LB) agar plates. Then, each group of hydrogels was placed on the agar plates and after 24 h of incubation, the inhibition zone was assessed. For testing the effects of hydrogels on the growth of bacteria, equal volumes of hydrogels from each group (Gel/CS-Au_5, Gel/CS-Au_{10}, Gel/CS-Au_{25}, and Gel/CS-Au_{50}) and PBS (control) were added into the wells of a 24-well microplate. Subsequently, 1 mL of *E. coli, S. aureus*, and *MRSA* bacterial suspensions (10^7 to 10^8 CFU/mL) were added to each well. Following a 12-hour incubation, the bacterial solution was aspirated, and the bacteria were subsequently diluted 10^4-fold. The diluted solution was then pipetted onto LB agar plates and further incubated for 12 h at 37°C. The growth of bacteria in each group was checked and photographed by a camera and the total number of colonies were counted. To further explore the antibacterial properties of the hydrogel dressing, bacterial suspension (10^9 CFU/mL) was transferred to sterilized 12-well plates. Then, sterilized Gel/CS-AuNPs were mixed with the bacterial suspension and incubated for 24 h. Subsequently, the prepared bacteria were then stained with the LIVE/DEAD BacLight Bacterial Viability Assay Kit and photographed using an inverted fluorescence microscope. A measured quantity of Gel/CS-Au_{25} was introduced into each of the three identical volumes of bacterial solutions. Following a 12 h incubation period in a 37°C incubator, the samples were meticulously prepared, adhering to the sample preparation methods detailed in established literature.[12] Subsequently, the samples underwent bacterial observation using SEM.

Generation of Type II Diabetic Model (TIIDM) Rats

The TIIDM rats were developed following established procedures.[5] Male Sprague-Dawley rats were accommodated in a standard SPF animal room at a temperature of 23 ± 2°C. After a one-week acclimation period, during which they were fed a standard diet, the rats were subjected to a high-fat diet for six weeks. After a 12-hour fasting period, the rats received an administration of 35 mg/kg streptozotocin (STZ). The model was deemed established when blood glucose levels reached ≥16.7 mmol/L on days 3 and 7. All procedures involving rats adhered to the guidelines provided by the Institutional Animal Care and Use Committee of Jilin University (Changchun, P. R. China, KT202203069).

In vivo Infected TIIDM Diabetic Wound Healing

A total of fifteen TIIDM rats were randomly allocated into five groups: (1) control, (2) Gel/CS-Au_5, (3) Gel/CS-Au_{10}, (4) Gel/CS-Au_{25}, and (5) Gel/CS-Au_{50}. All experimental procedures were performed under sterile conditions. TIIDM rats were anesthetized by inhalation of vapor containing 5% isoflurane and fixed on the operating table. After applying the depilatory agent, the hair was shaved from the back of the TIIDM rats. The exposed skin was sterilized. Then, the full-thickness skin on the back was cut with ophthalmic scissors to generate a wound of 1 cm diameter. An equal volume of *MRSA* (1×10^6 CFU, 200 μL PBS) was then inoculated on the wound surfaces to establish the TIIDM infected wound

model rats. We observed purulent exudates under the crusts on the wound surface at 24 h. Subsequently, after simple debridement with normal saline, the wounds were immediately covered with sterile Gel/CS-AuNPs. The control group was not given any special treatment. The wound dressing was changed every three days. To maintain stability, the wound was covered with a highly breathable medical vacuum sealing drainage membrane (VSD). The wounds were photographed on days 0, 6, 9, 12, and 15. The images underwent processing with Image J software, and the measurement of the wound area was conducted using the formula: Residual wound area (%) = $S_t/S_0 \times 100\%$, where S_0 denotes exposed area of the wound on day 0 and S_t denotes exposed area of the wound on days 6, 9, 12, and 15.

Histopathology and Immunofluorescence Staining

The experimental rats were euthanized on day 15. Following that, Section samples were prepared by extracting full-thickness skin tissue with a diameter of 1.5 cm from the wound center.[24] These sections were later stained using hematoxylin and eosin (H&E) as well as Masson's trichrome (MT) stains. The stained specimens were captured under a microscope, and Image J software was employed to evaluate both the thickness of the granulation tissue and collagen deposition. Immunofluorescence staining for TNF-α, IL-10, and CD31 was performed on the paraffin-embedded sections as previously described.[22] Fluorescence images were acquired using a confocal microscope and subsequently analyzed using Image J software.

Statistical Analysis

Differences among groups were assessed through one-way analysis of variance (ANOVA) using GraphPad Prism statistical software (Version 9.3, California, USA). Statistical significance was established at a P-value < 0.05. Histograms were generated, representing mean ± standard deviation values (n = 3). Significance indicators (*,#, Δ, and ◇) highlight comparisons: * denotes $P < 0.05$ compared with the control group, # denotes $P < 0.05$ compared with the Gel/CS-Au_5 group, Δ denotes $P < 0.05$ compared with the Gel/CS-Au_{10} group, and ◇ denotes $P < 0.05$ compared with the Gel/CS-Au_{25} group unless otherwise specified.

Results and Discussion

Basic Characterization of Gel/CS-AuNPs

AuNPs show good biocompatibility and are widely used as building blocks for various biomaterials.[10,11,25,26] Therefore, AuNPs self-assemble to form stable nanosystems. Functionalization improves the dispersion of AuNPs and confers better bioactivity. CS binds to negatively charged AuNPs through electrostatic interactions and self-assembles into functionally modified CS-AuNPs that can be loaded onto hydrogels. Figure 1 shows the scheme used in this study for the synthesis of Gel/CS-AuNPs and the in vivo analyses of their efficacy in healing bacteria-infected wounds in diabetic rats. TEM images showed that the AuNPs and CS-AuNPs were spherical with diameters of 14.15±1.02 nm and 14.89±1.38 nm, respectively (Figure 2A–C). Functionalization of AuNPs with CS did not alter their size and form. CS-modified AuNPs were spherical and showed high dispersion but aggregation was not observed. Figure 2D displays the XRD patterns of both AuNPs and CS-AuNPs. The XRD spectra of AuNPs revealed distinct diffraction peaks at 38.4°, 44.5°, and 64.3°, indicative of the (111), (200), and (220) crystalline planes of metallic Au, respectively.[27] The characteristic metallic peaks of CS-AuNPs also appeared at the same position as Au. Therefore, XRD data confirmed successful synthesis of AuNPs and CS-AuNPs. Then, we analyzed the absorption spectra of solutions (equal volumes) with 5% (CS-Au_5), 10% (CS-Au_{10}), 25% (CS-Au_{25}), and 50% (CS-Au_{50}) of the originally prepared CS-AuNPs using a UV-Vis spectrophotometer (Figure 2E). The surface plasma resonance absorbance peak for AuNP was observed at 520 nm. We observed a similar absorption peak at 520 nm for all the solutions with different concentrations of CS-AuNP. This demonstrated that the major absorption peak for CS-AuNPs was from AuNP. This further confirmed chemical synthesis of AuNP. The absorbance at 520 nm increased gradually with higher concentrations of CS-AuNPs (CS-Au_5 to CS-Au_{50}) and was maximum for the solution with the original concentration of the AuNPs. Zeta potential of the AuNPs was about −25 mV (Figure 2F). Then, after loading with CS, the zeta potential of the AuNPs increased to approximately +30 mV. This demonstrated electrostatic adsorption of CS onto the AuNPs, thereby providing a solid foundation for the antimicrobial mechanism of the material. As shown in Figure 2G, FTIR spectra of CS, CS- AuNPs, SA, Gelation, Gel, and a series of Gel/CS-AuNPs. The dense band of hydroxyl (-OH) oscillations of Gel/CS-Au_5, Gel/CS-Au_{10}, Gel/CS-Au_{25}, and Gel/CS-Au_{50} was red-shifted from the 3410 cm^{-1} to 3250 cm^{-1} as compared to the

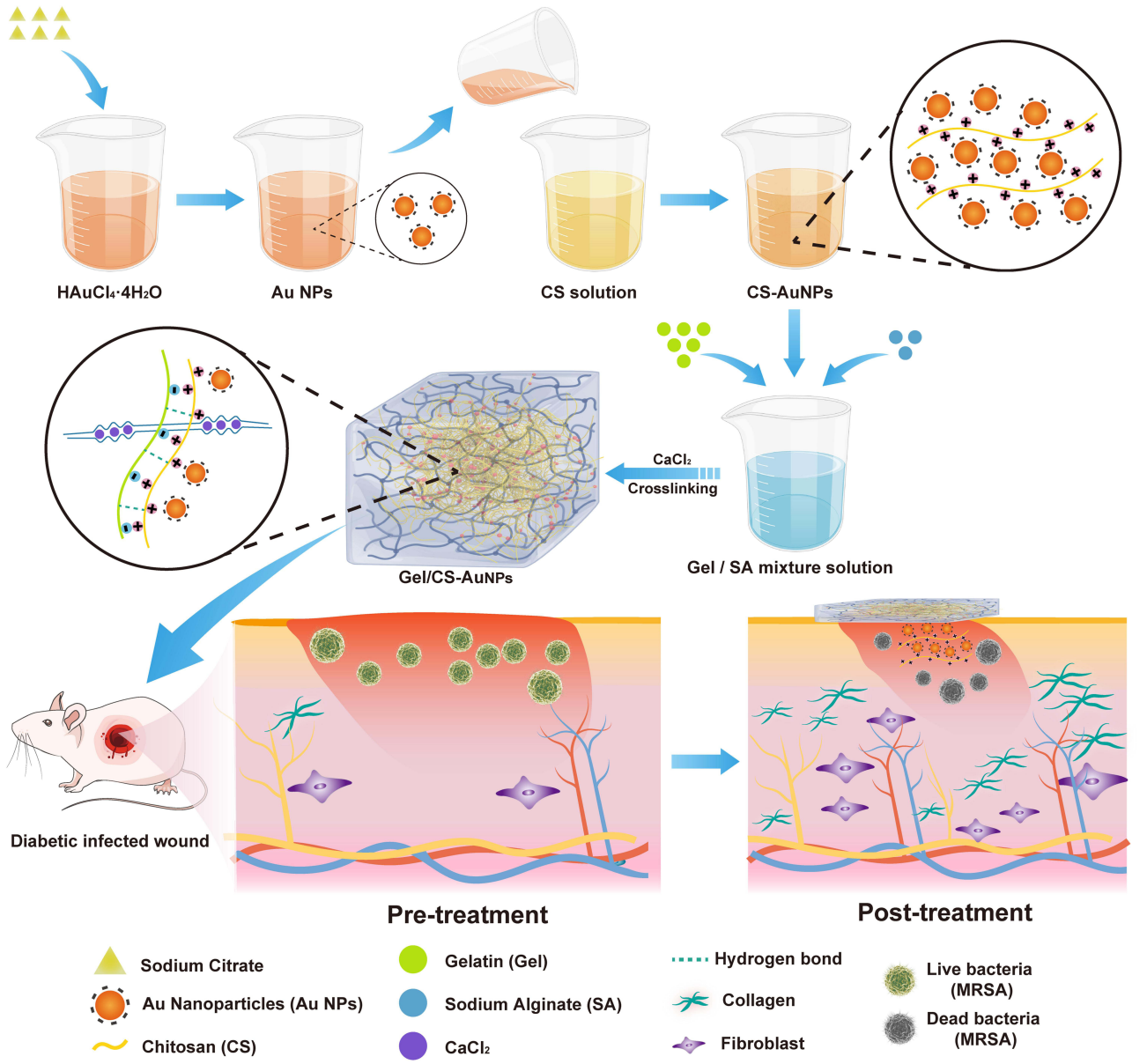

Figure 1 Schematic representation shows the synthesis of Gel/CS-AuNPs and experimental strategy for assessing their efficacy in healing the infected diabetic wounds in the rat model.

FT-IR spectra of CS.[28] The location and size of the spectral peaks demonstrated that hydroxyl group (-OH) in the hydrogel participated in the formation of hydrogen bonds between neighboring molecules. Moreover, compared with the CS spectra, the amino bands of CS-AuNPs, Gel/CS-Au_5, Gel/CS-Au_{10}, Gel/CS-Au_{25}, and Gel/CS-Au_{50} are red-shifted from ~1660 cm^{-1} to ~1620 cm^{-1} in the presence of AuNPs due to electrostatic interactions between the amino group and the AuNPs.[29] Gelatin exhibited distinctive features, including an amine band at 1520 cm^{-1} and a carbonyl peak at 1620 cm^{-1}.[30] The peak near 1020 cm^{-1} (C-O-C stretching) in the SA sample was attributed to the sugar structure. In the spectra of composite hydrogels, distinct combinatorial peak patterns were observed for gelatin, SA, and CS-AuNPs, thereby suggesting the existence of all these three polymers in Gel/CS-Au_5, Gel/CS-Au_{10}, Gel/CS-Au_{25}, and Gel/CS-Au_{50}.[30]

Spectral and Electron Microscopic Analysis of Gel/CS-AuNPs

SEM image analysis of the hydrogels showed that the pore sizes of Gel (Gelatin/SA), Gel/CS-Au_5, Gel/CS-Au_{10}, Gel/CS-Au_{25}, and Gel/CS-Au_{50} were 207.43 ± 40.09 μm, 226.82 ± 17.83 μm, 217.61 ± 30.66 μm, 232.03 ± 29.83μm, 227.82

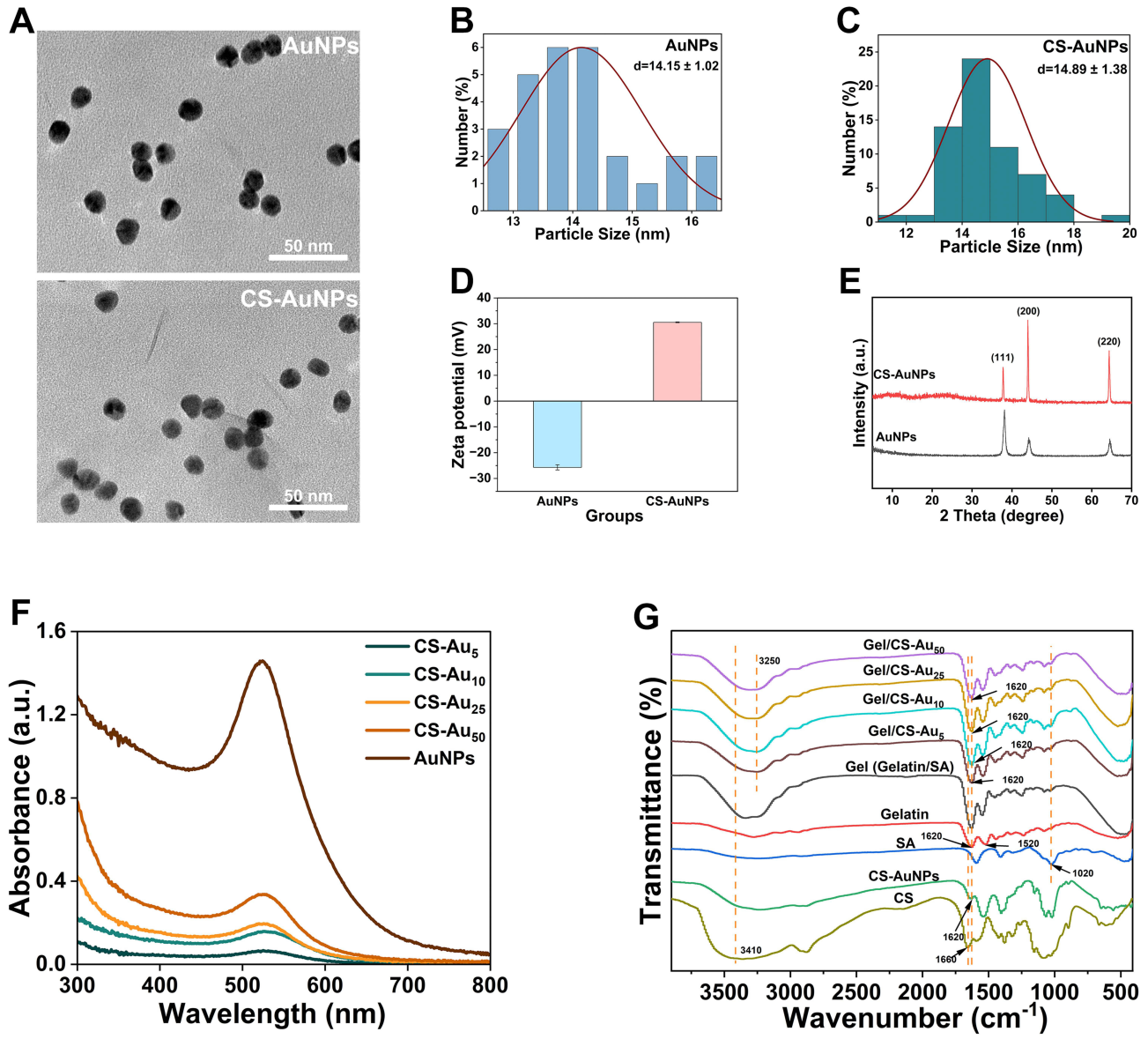

Figure 2 Basic characterization of CS-AuNPs. (**A**) TEM images of AuNPs and CS-AuNPs. Scale bars: 50 nm. (**B** and **C**) Histograms show the size distribution of AuNPs and CS-AuNPs. (**D**) Zeta potential of AuNPs and CS-AuNPs (n=3). (**E**) XRD spectra of AuNPs and CS-AuNPs. Zeta potential of AuNPs and CS-AuNPs (n=3). (**F**) UV-visible spectra of AuNPs, CS-Au_5, CS-Au_{10}, CS-Au_{25}, and CS-Au_{50}. (**G**) FT-IR spectra of CS, CS-AuNPs, SA, Gelatin, Gel (Gelatin/SA), Gel/CS-Au_5, Gel/CS-Au_{10}, Gel/CS-Au_{25}, and Gel/CS-Au_{50}.

± 26.56 μm, respectively, based on the SEM image analysis of the hydrogels (Figure 3A). This demonstrated that the pores of all the five groups of hydrogels were larger than 200 μm. The pore structure of the hydrogels promoted the release of CS-AuNPs. We then performed EDS mapping to evaluate the distribution of elements on Gel/CS-Au_{25} in the canonical case. The elemental mapping relationships of C, N, O, and Au are shown in Figure 3B. These images showed that the AuNPs were uniformly distributed throughout the hydrogels and also further validated the presence of Au.

Rheological Features of Gel/CS-AuNPs

The mechanical parameters of hydrogels were determined by measuring the G' and G" of each group of hydrogels. As shown in Figure 3C, the G' values in all hydrogel samples showed a small and steady increase as the oscillation frequency increased from 1 to 100 rad/s. This observation indicates the consistent stability of the mechanical properties exhibited by the hydrogels. Furthermore, G′ values were larger than the G″ values for all the groups of hydrogels. This

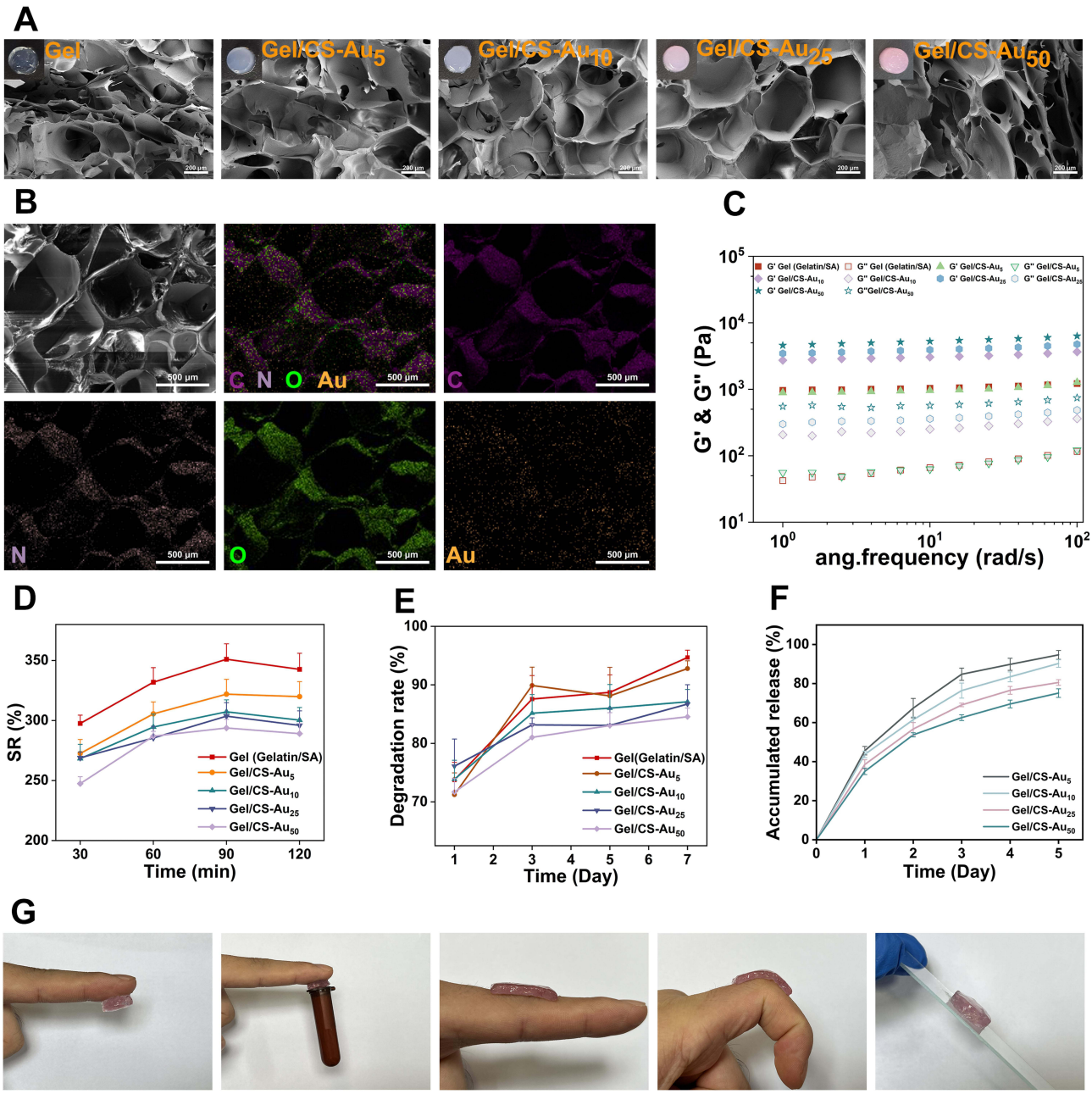

Figure 3 Basic characterization of Gel/CS-AuNPs. (**A**) Representative SEM images of Gel, Gel/CS-Au_5, Gel/CS-Au_{10}, Gel/CS-Au_{25}, and Gel/CS-Au_{50}. Scale bars: 200 μm. (**B**) EDS mapping images of C, N, O, and Au in Gel/CS-Au_{25}. Scale bars: 500 μm. (**C**) Determination of rheological properties of hydrogels. (**D**) The swelling rate (SR %) analysis of Gel, Gel/CS-Au_5, Gel/CS-Au_{10}, Gel/CS-Au_{25}, and Gel/CS-Au_{50}. SR was evaluated by recording change in the wet weight during incubation with PBS for 30, 60, 90, and 120 minutes (n = 3). (**E**) The in vitro degradation rate of Gel, Gel/CS-Au_5, Gel/CS-Au_{10}, Gel/CS-Au_{25}, and Gel/CS-Au_{50} (n = 3). (**F**) The in vitro accumulated release amount of CS-AuNPs from each group of hydrogels (n = 3). (**G**) Sample pictures show the adhesive properties of the hydrogels.

observation indicates the high elasticity of the hydrogels, consistently maintaining a stable hydrogel state. The G′ values of the Gel/CS-AuNPs increased with the CS-AuNPs content of the hydrogels. This suggested that the CS-AuNPs enhanced the elasticity of hydrogels.

Swelling Features of Gel/CS-AuNPs

We analyzed the swelling features of the hydrogels under physiological settings in PBS at 37°C. The hydrogels in all the groups reached equilibrium in 120 minutes. SR was highest for the Gel (Gelatin/SA) at 350%. SR showed a decreasing trend with increasing concentration of the CS-AuNPs. This suggested that the CS-AuNPs concentration affected the swelling of hydrogels.

Overall, the swelling of all the hydrogel groups was high and the SR values were > 260% (Figure 3D). These experiments demonstrated that the water absorption ability of the hydrogels was high. Consequently, these hydrogels effectively soak up considerable inflammatory exudates from diabetic wounds, preventing their accumulation around the wound.[31] This process accelerates the diabetic wound healing, positioning the hydrogel as a potential ideal dressing for diabetic wounds.

Biodegradability of Gel/CS-AuNPs

Degradability of hydrogels is an essential parameter for considering whether they can be used to load the CS-AuNPs for wound dressing. The in vitro degradability of the hydrogels was assessed by measuring the dry weight change of the hydrogels under physiological conditions. As indicated in Figure 3E, degradation rate for all the groups of hydrogels was > 80% in three days. Gel (Gelatin/SA) showed the best effect with a degradation rate of >95% within seven days. Degradation rate was reduced with increasing concentration of CS-AuNPs. Overall, the degradation effect of the hydrogels in all the groups was high and significant. Therefore, hydrogels showed excellent degradation properties and could efficiently release CS-AuNPs during the experimental process. Furthermore, the materials of hydrogels could be removed easily, thereby further improving healing of the diabetic wounds.

Release of CS-AuNPs from the Hydrogels

The release of CS-AuNPs from hydrogels assumes a pivotal role in antimicrobial effects, prompting an exploration of their release dynamics across distinct hydrogel groups. The outcomes are illustrated in Figure 3F. Notably, within the initial three days, CS-AuNPs within each hydrogel group underwent a phase of rapid release, culminating in accumulated release rates of 84.76%, 76.39%, 69.04%, and 62.54% on the third day, respectively. After day 3, the release of CS-AuNPs decelerated, nearing equilibrium by day 5. The accumulated release rates on day 5 were 94.68%, 90.26%, 80.54%, and 75.09%, signifying a comprehensive release of CS-AuNPs from each hydrogel group. Remarkably, Gel/CS-Au_{25} and Gel/CS-Au_{50} exhibited comparatively subdued release rates compared to Gel/CS-Au_5 and Gel/CS-$Au_{10,}$ underscoring a discernible dose-related pattern in the CS-AuNPs release kinetics from hydrogels. The inherent hydrogel architecture, characterized by pores exceeding 200 μm and a heightened degradation rate, further expedited the release of CS-AuNPs from the hydrogel matrix. This accelerated release not only ensures sustained bioactivity of CS-AuNPs but also substantiates their potential in promoting therapeutic efficacy for bacterial-infected diabetic wounds.

Adhesive Properties of Gel/CS-AuNPs

As indicated in Figure 3G, the hydrogels attached to the fingertips without peeling. At the same time, the hydrogels were fixed on the dynamic skin surface and at the interphalangeal joints, the hydrogels did not move when the hand moved. This demonstrated that the hydrogels displayed tissue adhesiveness on hand skin. Moreover, the hydrogels could adhere to different materials, including glass plates. This further demonstrated that the hydrogels possessed a suitable degree of adhesion.[3,32] This suggested that adhesion of the wound dressing to the tissue would prevent the wound dressing from coming off, thereby helping to avoid exposure of the wound. This would reduce the frequency of changing the wound dressing and decrease additional damage to the wound.[20]

Gel/CS-AuNPs Show Significantly High in-vitro Cytocompatibility

Adequate biocompatibility is essential for the clinical implementation of biomaterials.[33–35] This study evaluated the cytocompatibility of the Gel/CS-AuNPs with different percentages of CS-AuNPs by co-culturing the extracts with NIH3T3 cells. NIH3T3 cells proliferation in various groups was assessed through the CCK-8 assay. As shown in Figure 4A, proliferation of the NIH3T3 cells increased significantly after 1, 3, and 5 days of co-culturing, however, no substantial differences were observed in the proliferation of NIH3T3 cells among the Gel/CS-Au_5, Gel/CS-$Au_{10,}$ Gel/CS-Au_{25}, and control groups. Nevertheless, the proliferation of NIH3T3 cells in the Gel/CS-Au_{50} group exhibited a lower rate compared to the control groups. This indicated that higher concentrations of CS-AuNPs in the Gel/CS-AuNPs inhibited cell proliferation; however, the viability of NIH3T3 cells in the Gel/CS-Au_{50} group was above 80% (Figure 4B). The results suggest good biocompatibility of the hydrogel, even at the highest concentration tested in the experiments. Subsequently, an examination of the impact of hydrogel materials on NIH3T3 cell viability was conducted through live/dead cell staining. As depicted in Figure 4C, the majority of NIH3T3 cells in the

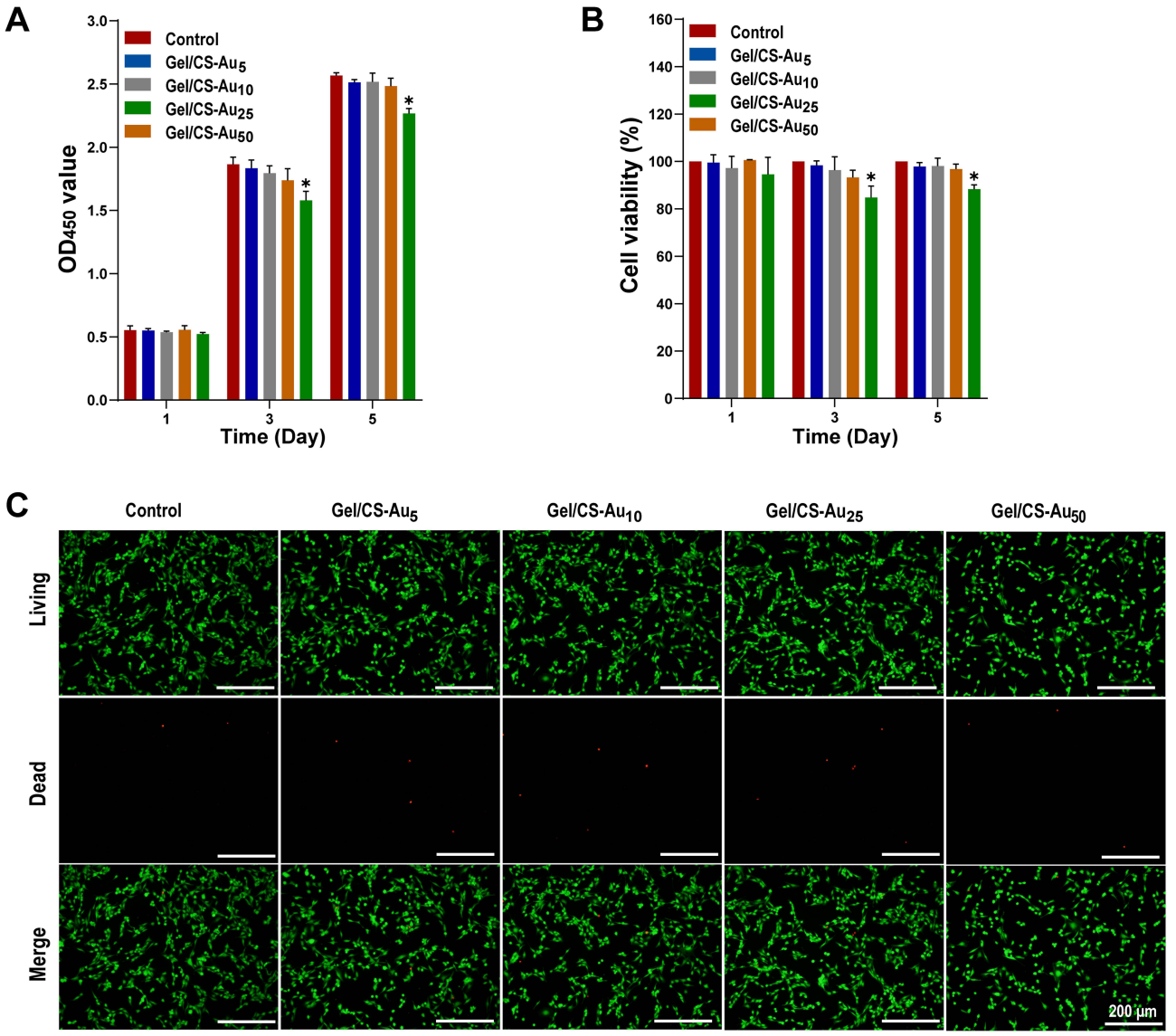

Figure 4 In vitro effects of Gel/CS-AuNPs on NIH3T3 cell proliferation and viability. (**A**) CCK-8 assay results show the proliferation of NIH3T3 cells after incubation with Gel, Gel/CS-Au_5, Gel/CS-Au_{10}, Gel/CS-Au_{25}, and Gel/CS-Au_{50} on days 1, 3, and 5 (n = 3). (**B**) Estimation of NIH3T3 cell viability after incubation with Gel, Gel/CS-Au_5, Gel/CS-Au_{10}, Gel/CS-Au_{25}, and Gel/CS-Au_{50} on days 1, 3, 5, and 7. (**C**) Live/dead NIH/3T3 cell staining results after incubation with Gel, Gel/CS-Au_5, Gel/CS-Au_{10}, Gel/CS-Au_{25}, and Gel/CS-Au_{50} for 1, 3, and 5 days (n = 3). (*Denotes $P < 0.05$ compared with the control group).

experimental groups exhibited vitality (green fluorescence) and displayed a spindle shape. Notably, the Gel/CS-Au_{50} group showed a slightly diminished number of viable cells compared to other experimental groups, aligning with the findings from the CCK-8 assay.

Gel/CS-AuNPs Show Significantly High in-vitro Antimicrobial Activity

The high glucose environment and a large amount of exudate around the diabetic wounds provides a suitable medium for persistent bacterial infections and leads to excessive inflammatory response.[4] Therefore, hydrogel dressings with good antibacterial properties are of immense value for healing infected wounds in diabetic patients. Free AuNPs do not possess any antibacterial activity. However, antibacterial property of the AuNPs can be activated through ligand modifications. Ligand-modified AuNPs are cytotoxic to the bacteria because they disrupt the integrity of bacterial membrane by interacting with the surface ligands on the bacterial cell membrane, thereby penetrating the bacterial cell and altering the structure of the bacterial components.[11,36] In this study, we investigated the antibacterial activity of Gel/CS-AuNPs against *E. coli, S. aureus*, and *MRSA*. The treatment groups exhibited a notable reduction in the number of bacterial colonies compared to the control group. Specifically,

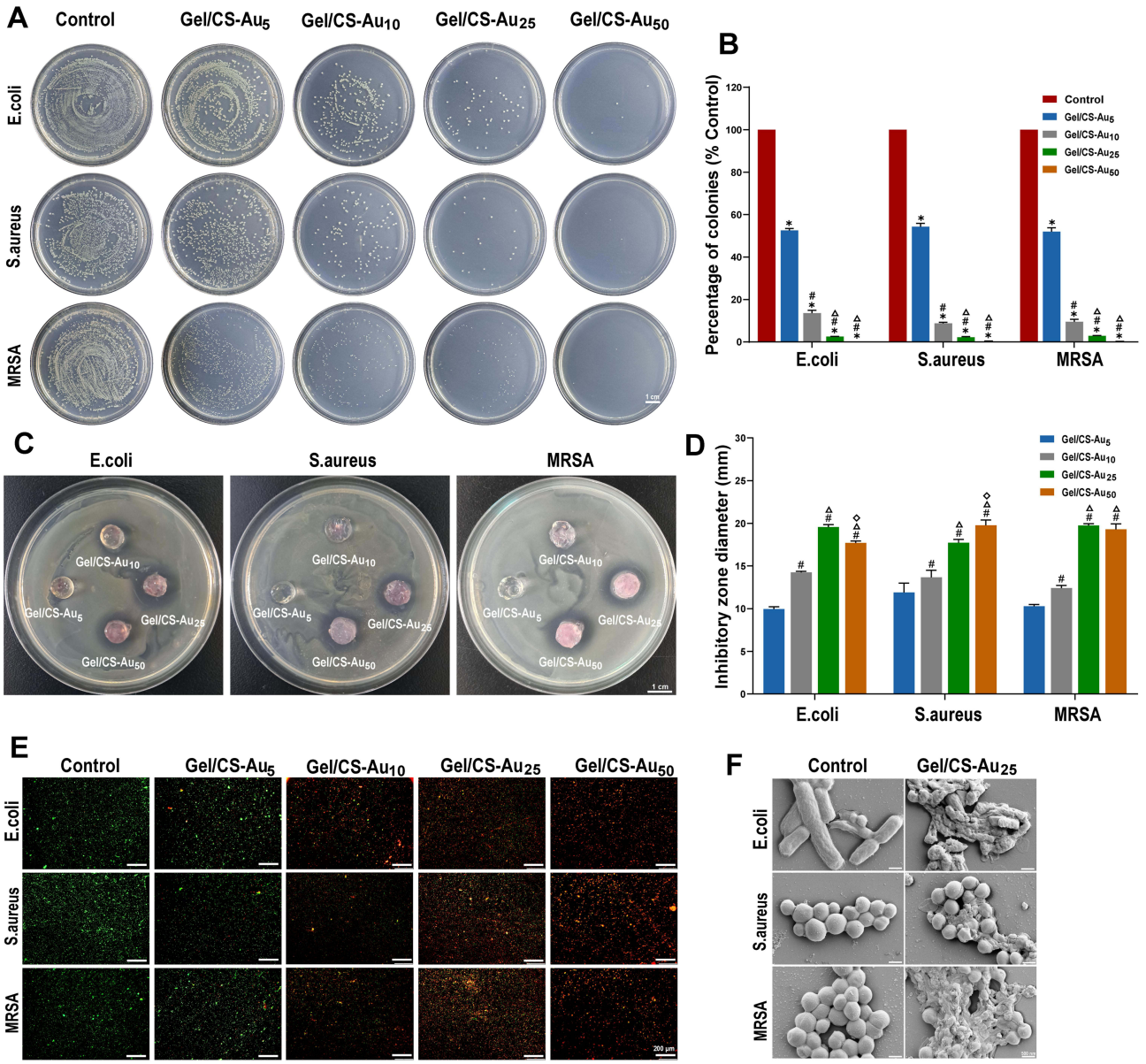

Figure 5 In vitro antimicrobial activity of Gel/CS-AuNPs. (**A**) Sample pictures show agar plates with colonies of *E. coli, S. aureus*, and *MRSA* after treatment with control, Gel/CS-Au_5, Gel/CS-Au_{10}, Gel/CS-Au_{25}, and Gel/CS-Au_{50}. Scale bars: 3 cm. (**B**) Histograms show the percentage of *E. coli, S. aureus*, and *MRSA* colonies after treatment with control, Gel/CS-Au_5, Gel/CS-Au_{10}, Gel/CS-Au_{25}, and Gel/CS-Au_{50}. (**C**) Representative images show the *E. coli, S. aureus*, and *MRSA* suppression rings after treatment with Gel/CS-Au_5, Gel/CS-Au_{10}, Gel/CS-Au_{25}, and Gel/CS-Au_{50}. Scale bars: 3 cm. (**D**) Quantitative analysis of the *E. coli, S. aureus*, and *MRSA* suppression ring diameter after treatment with Gel/CS-Au_5, Gel/CS-Au_{10}, Gel/CS-Au_{25}, and Gel/CS-Au_{50}. (**E**) Live/dead imaging analysis photographs of *E. coli, S. aureus*, and *MRSA* after treatment with control, Gel/CS-Au_5, Gel/CS-Au_{10}, Gel/CS-Au_{25}, and Gel/CS-Au_{50}. Scale bars: 200 μm. (**F**) SEM images of *E. coli, S. aureus* and *MRSA* after treatment with Gel/CS-Au_{25} for 12 h. Histograms were plotted with the mean ± standard deviation values (n = 3) (*Denotes $P < 0.05$ compared with the control group; $^{\#}$Denotes $P < 0.05$ compared with the Gel/CS-Au_5 group; $^{\Delta}$Denotes $P < 0.05$ compared with the Gel/CS-Au_{10} group; $^{\diamond}$Denotes $P < 0.05$ compared with the Gel/CS-Au_{25} group).

the Gel/CS-Au_{25} and Gel/CS-Au_{50} groups demonstrated significantly enhanced antibacterial properties in comparison to the Gel/CS-Au_5 and Gel/CS-Au_{10} groups, as illustrated in Figure 5A and B. The antibacterial effects of Gel/CS-Au_{25} and Gel/CS-Au_{50} against gram-negative bacteria were significantly higher than those of Gel/CS-Au_5 and Gel/CS-Au_{10} (Figure 5C and D). The antibacterial ring test results further confirmed the bactericidal effects of different Gel/CS-AuNPs groups against the gram-positive bacteria and *MRSA*. The bacterial live-death assay results showed that the bactericidal effects of the Gel/CS-AuNPs treatment groups were higher than the control group (red); moreover, the Gel/CS-Au_{25} and Gel/CS-Au_{50} groups showed higher bactericidal effects than the other groups (Figure 5E). To delve deeper into the antibacterial mechanism of CS-AuNPs, Gel/CS-Au_{25}, known for its heightened antibacterial efficacy, was employed in co-cultivation with *E. coli, S. aureus*, and *MRSA* for 24 h. Subsequently, the bacterial fluids were processed into samples and subjected to SEM observation. As depicted in Figure 5F, the

morphology of all three bacterial strains underwent significant disruption, characterized by cell membrane collapse and rupture. These findings offer further confirmation that CS-AuNPs possess the capability to sterilize bacteria through the disruption of their cell membranes. This phenomenon is closely associated with the positive charge on the surface of CS-AuNPs and their ensuing electrostatic interaction with bacteria.

Gel/CS-AuNPs Effectively Promote Healing of Diabetic Infected Wounds

The images of the wounds from different groups of diabetic model rats and the changes in the wound sizes in the control and treatment groups rats at all time points (day 0, 6, 9, 12, and 15) are shown in Figure 6A–C. We did not observe wound-healing in the control group at all time points, whereas regeneration of the skin epithelium in the wound area and significant wound-healing effects were observed in all the treatment groups. On day 6, the wound area of the control group was 92.8%, whereas the wound areas of the four treatment groups were 80.5%, 65.4%, 50.7%, and 61.7%, respectively. The treatment groups showed significantly better wound healing than the control group. The Gel/CS-Au_{25} group showed highest degree of wound healing than the other treatment groups on days 9 and 12. After 15 days of treatment, only 3.1% of the wound area remained in the Gel/CS-Au_{25} group. Therefore, the treatment effect was significant in the Gel/CS-Au_{25} group and the wound was almost completely healed. This outcome may be correlated with the capacity of Gel/CS-AuNPs to proficiently eliminate *MRSA* infection and absorb wound exudates, consequently leading to a reduction in the inflammatory response within the wound area. Moreover, wound healing effect was dependent on the dose of the CS-AuNPs. Besides, prolonged retention of higher concentrations of CS-AuNPs in the wounds of the Gel/CS-Au_{50} group may have inhibited wound tissue regeneration through inflammatory or immune responses.[37]

Wound healing is a complex and highly coordinated process in the body that includes the following four stages: hemostasis, inflammation, hyperplasia (granulation), and remodeling.[38,39] We used H&E and MT staining to evaluate the extent of wound re-epithelialization and the quality of collagen deposition histologically. Figure 6D illustrates the migration of keratinocytes toward the wound site, culminating in the establishment of a new epithelial layer at the wound edge. Regeneration of the epithelium was absent or insignificant in the control group, but significant epithelial regeneration was observed in the treatment groups. Compared with the control group, the dermal gap lengths in the treatment groups were significantly reduced (red arrow), and the variances from the control group were found to be statistically significant ($P<0.05$). In the Gel/CS-Au_{25} group, the dermal space exhibited the lowest length, accompanied by nearly complete epithelial tissue regeneration. The boundary of the epidermal layer (indicated by yellow dashed lines) and the dermis was distinctly clear. Moreover, within the wound area, the regenerated epithelium displayed characteristics resembling normal epithelial tissue, complete with skin appendages such as hair follicles and sebaceous glands (indicated by black arrow). Notably, Gel/CS-Au_{25} demonstrated effective promotion of epithelial regeneration, expediting the overall wound healing process. This observation aligns with the findings regarding the residual wound area ratio. The thickness of the granulation tissue serves as a crucial metric for assessing the extent of wound healing. As depicted in Figure 6D (shown by yellow arrow) and Figure 6F, the thickness of granulation tissue in the treatment groups exhibited a significant increase compared to the control group. This suggested that CS-AuNPs promoted cell migration and proliferation, which are closely related with effective control of infection and reduced inflammation. In the Gel/CS-Au_{25} group, the thickness of granulation tissue was highest and showed a large number of new blood vessels and a prominent vascular lumen structure (green arrow). This suggested that the cells at the site of the wound area were actively proliferating in the Gel/CS-Au_{25} group. However, compared with the Gel/CS-Au_{25} group, the Gel/CS-Au_{50} group with a higher CS-AuNPs concentration showed lower granulation tissue thickness and neovascularization. Furthermore, skin appendages were not observed in the new epithelium of the Gel/CS-Au_{50} group. As demonstrated in the preceding cell proliferation experiments, the heightened concentration of CS-AuNPs in the Gel/CS-Au_{50} group exhibited an inhibitory effect on fibroblast proliferation. Consequently, we posit that the increased concentration of CS-AuNPs in the Gel/CS-Au_{50} group may have impeded local tissue regeneration to some extent.

Within the dermal extracellular matrix (ECM), collagen stands as a primary constituent, playing a pivotal role in the reorganization and remodeling of the ECM and tissue.[40,41] We analyzed collagen deposition by MT staining. The collagen content exhibited a significant increase in all treatment groups when compared to the control group

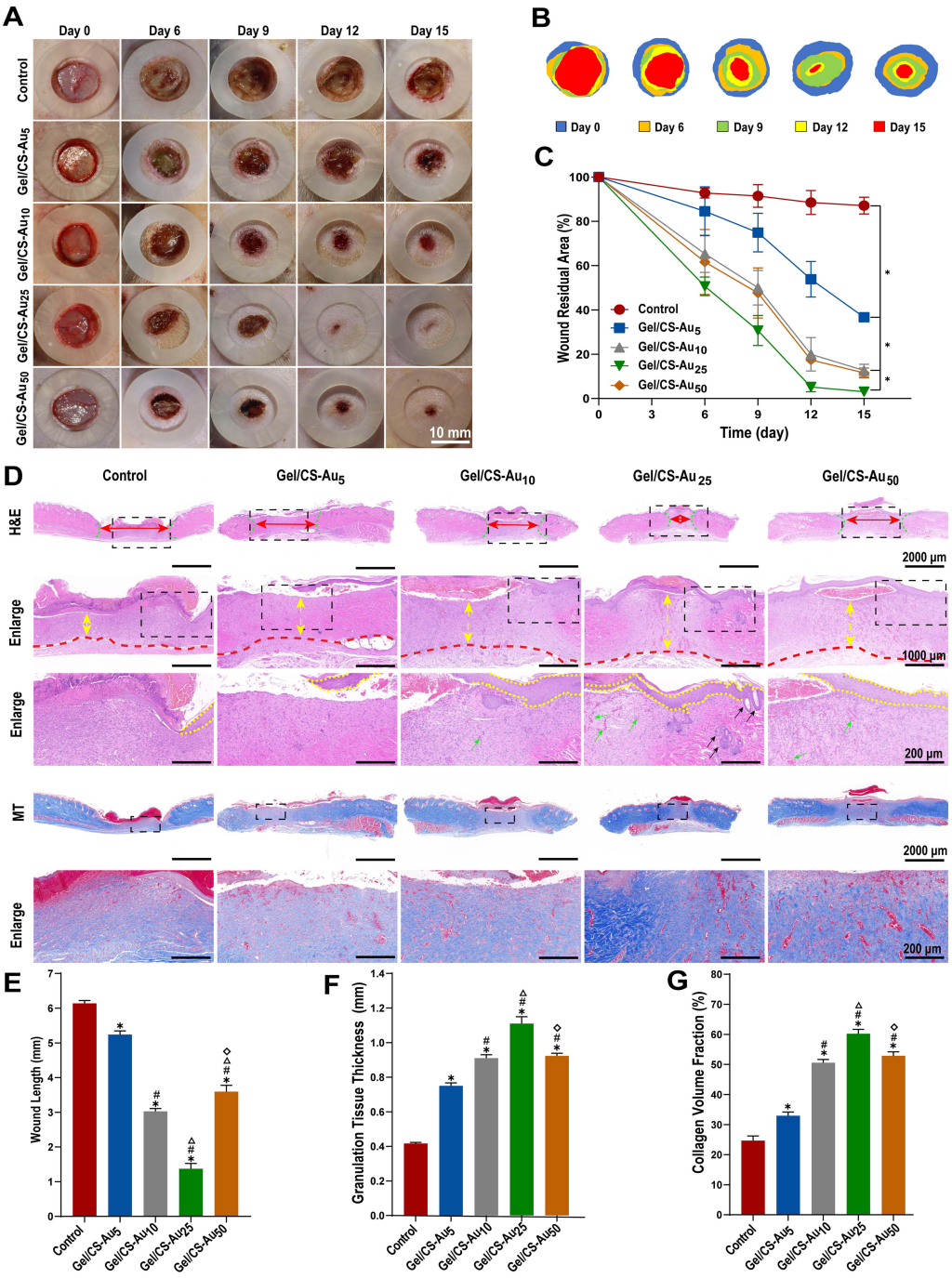

Figure 6 In vivo effects of Gel/CS-AuNPs on accelerated healing of diabetic wounds in the rat model. (**A**) Sample pictures show the wound bed on days 0, 6, 9, 12, and 15 in the TIIDM rats belonging to the control, Gel/CS-Au_5, Gel/CS-Au_{10}, Gel/CS-Au_{25}, and Gel/CS-Au_{50} groups. Scale bars: 10 mm. (**B**) Wound traces on days 0, 6, 9, 12, and 15. (**C**) The line plot shows the changes in the wound residual area (%) in the TIIDM rats belonging to the control, Gel/CS-Au_5, Gel/CS-Au_{10}, Gel/CS-Au_{25}, and Gel/CS-Au_{50} groups on days 0, 6, 9, 12, and 15. (**D**) Sample pictures show H&E- and MT-stained sections of wounds from the TIIDM rats belonging to the control, Gel/CS-Au_5, Gel/CS-Au_{10}, Gel/CS-Au_{25}, and Gel/CS-Au_{50} groups. Scale bars: 2000 μm; 1000 μm; 200 μm. Red arrow shows wound length. Black dashed box shows the boxed part is enlarged. Green dashed curve shows the dermal tissue boundary at the wound. Yellow arrow shows granulation tissue thickness. Red dashed lines show granulation tissue border. Yellow dashed lines show the boundary of the epidermal layer. Green arrow shows neovascularization. Black arrow shows skin appendages. (**E**) Histograms show the wound lengths based on H&E staining in the TIIDM rats belonging to the control, Gel/CS-Au_5, Gel/CS-Au_{10}, Gel/CS-Au_{25}, and Gel/CS-Au_{50} groups. (**F**) Histogram shows the thickness of granulation tissue in the TIIDM rats belonging to the control, Gel/CS-Au_5, Gel/CS-Au_{10}, Gel/CS-Au_{25}, and Gel/CS-Au_{50} groups. (**G**) Histogram shows the mean collagen deposition in the wound areas of the TIIDM rats belonging to the control, Gel/CS-Au_5, Gel/CS-Au_{10}, Gel/CS-Au_{25}, and Gel/CS-Au_{50} groups. Mean deposition of collagen was based on the specific fluorescent density per field viewpoint. Histograms were plotted with the mean ± standard deviation values (n = 3) (*Denotes $P < 0.05$ compared with the control group; #Denotes $P < 0.05$ compared with the Gel/CS-Au_5 group; △Denotes $P < 0.05$ compared with the Gel/CS-Au_{10} group; ◇Denotes $P < 0.05$ compared with the Gel/CS-Au_{25} group).

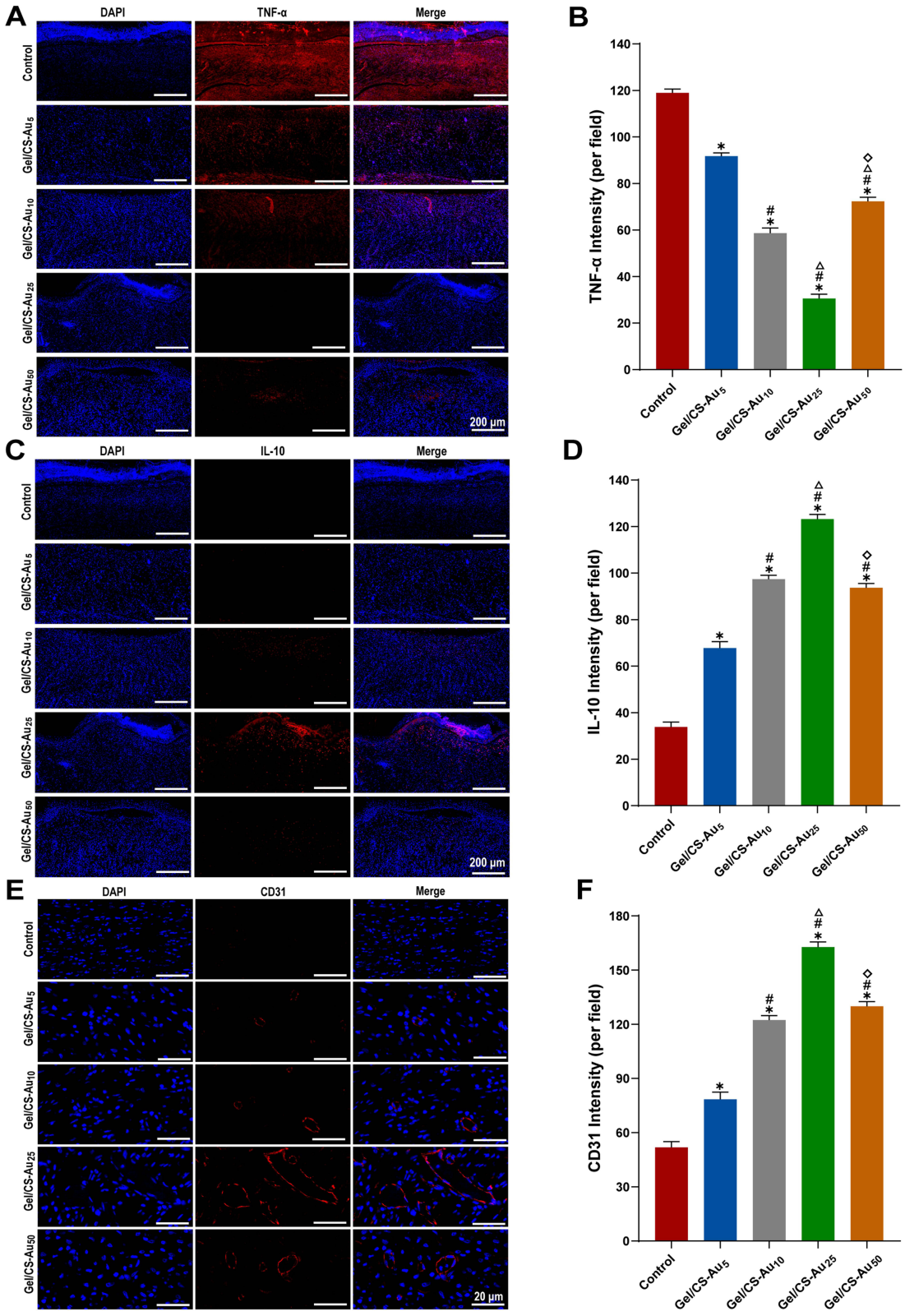

Figure 7 In vivo effects of Gel/CS-AuNPs on inflammatory response and neovascularization of diabetic wounds. (**A**) Immunofluorescence images the expression of the pro-inflammatory cytokine TNF-α. Scar bars:200 μm. (**B**) Mean fluorescence density per field of view for TNF-α. (**C**) Immunofluorescence images the expression of anti-inflammatory cytokine IL-10. Scar bars: 200 μm. (**D**) Mean fluorescence density per field of view for IL-10. (**E**) Immunofluorescence images the expression of CD31. Scale bars: 20 μm. (**F**) Mean fluorescence density per field of view for CD31. Histograms were plotted with the mean ± standard deviation values (n = 3) (*Denotes $P < 0.05$ compared with the control group; #Denotes $P < 0.05$ compared with the Gel/CS-Au_5 group; △Denotes $P < 0.05$ compared with the Gel/CS-Au_{10} group; ◇Denotes $P < 0.05$ compared with the Gel/CS-Au_{25} group).

https://doi.org/10.2147/IJN.S448282 DovePress

(Figure 6D and G). These results showed that the Gel/CS-AuNPs promoted collagen deposition. Bacterial infection has the potential to induce collagen damage within the granulation group, thereby impeding the process of wound healing.[42] This was related with the control of bacterial infection by the CS-AuNPs, which further promoted cell growth and collagen formation. In the Gel/CS-Au_{25} group, collagen fibers exhibited a higher density, darker, and more compact arrangement, closely resembling the characteristics of normal skin tissue. This demonstrated that Gel/CS-Au_{25} promoted collagen deposition and ECM remodeling. In conclusion, Gel/CS-Au_{25} promoted angiogenesis, epithelialization, and collagen deposition and remodeling by effectively controlling bacterial infection, reducing local inflammation, thereby accelerating healing of infected diabetic wounds.

Gel/CS-AuNPs Promote Diabetic Infected Wounds Healing by Decreasing Inflammation and Promoting Angiogenesis

The persistent release of a multitude of inflammatory factors resulting from bacterial infection places diabetic wounds in an inflammatory state, setting off a chain reaction within the body. This cascade hampers neovascularization, disrupts cell proliferation, and impedes the progression into the proliferative phase, thereby constituting a primary factor contributing to the development of chronic wounds.[38,43,44] As shown in Figure 7A–D, immunofluorescence analyses showed that the expression levels of TNF-α, a pro-inflammatory factor, were significantly lower at the wound sites of the treatment groups compared to the control group. In contrast, the expression levels of IL-10, an anti-inflammatory factor, were significantly higher at the wound site in the four treatment groups ($P < 0.05$). These findings indicate that the Gel/CS-AuNPs accelerated wound healing by decreasing the inflammatory response at the wound site by controlling bacterial infection. Among the treatment groups, the Gel/CS-Au_{25} group showed the lowest TNF-α levels and the highest IL-10 concentration. This suggested that the anti-inflammatory effect was significantly higher in the Gel/CS-Au_{25} group. TNF-α levels were higher in the Gel/CS-Au_{50} group compared with the Gel/CS-Au_{10} and Gel/CS-Au_{25} groups. This may be caused by increased inflammatory response because of excessive accumulation of the CS-AuNPs at the wound site in the Gel/CS-Au_{50} group. This may also contribute to reduced wound healing in the Gel/CS-Au_{50} group.

Neovascularization promotes infiltration of macrophages and monocytes to the wound site, thereby delivering growth factors, nutrients, oxygen, and other essential substances for wound healing.[45,46] Therefore, diabetic wound healing can be accelerated by promoting angiogenesis. Illustrated in Figure 7E and F, the treatment groups demonstrated significantly heightened CD31 expression levels compared to the control group. This suggested increased angiogenesis in the treatment groups. Furthermore, CD31 expression levels were highest in the Gel/CS-Au_{25} group among the treatment groups. This demonstrated that neovascularization was most effective in the Gel/CS-Au_{25} group and was consistent with the results of H&E staining. This demonstrated that CS-AuNPs effectively eliminated the bacteria, inhibited excessive inflammatory response, and promoted macrophage-associated immune regulation, angiogenesis, cell proliferation and tissue repair.

Conclusions

Treating diabetic wounds becomes more challenging due to antibiotic-resistant bacterial infections. We explored a novel antimicrobial strategy using metal nanoparticles. Since free AuNPs lack antimicrobial ability, we successfully modified them by electrostatically adsorbing CS onto AuNPs, resulting in significant antimicrobial activity. By incorporating CS-AuNPs into hydrogels, we achieved a slow release of CS-AuNPs for wound protection, along with the absorption of wound exudate to enhance the promotion of wound healing. Gel/CS-AuNPs accelerated wound healing through a dose-dependent increase in the bactericidal effects, enhanced angiogenesis, reduced inflammation, and increased collagen deposition and epithelial regeneration. Gel/CS-Au_{25} group showed the highest therapeutic effect and has great promise in clinical applications, including treatment of diabetic wounds infected by antibiotic-resistant bacteria. The preparation process of Gel/CS-AuNPs was simple and cost-effective. It did not require substantial amounts of energy and expensive chemical drugs. Therefore, Gel/CS-AuNPs have excellent commercial and clinical application possibilities, including treatment of diabetic wounds as shown in this study.

Ethics Approval and Consent

The use of experimental animals in this study has been approved by the Institutional Animal Care and Use Committee of Jilin University. All procedures strictly adhere to the guidelines for the care and utilization of experimental animals set forth by Jilin University.

Acknowledgments

This research received financial support from the National Natural Science Foundation of China under Grant/Award Number 81901365, the Department of Finance of Jilin Province with Grant/Award Number 2020SCZT051, and the Jilin Science and Technology Agency through Grants/Award Numbers YDZJ202201ZYTS572, YDZJ202201ZYTS071, and 20210402001GH. This work additionally received support from the Heilongjiang Natural Science Foundation of China under Grant/Award Number JQ2021H004. The authors express their gratitude to Ms. Zhengxian Xu (from Bengbu Medical University), Mr. Huidong Zhou and Dr. Rui Li (from the Second Hospital of Jilin University) for their valuable contributions to the study.

Disclosure

The authors declare no conflicts of interest in this work.

References

1. Saeedi P, Petersohn I, Salpea P, et al. Global and regional diabetes prevalence estimates for 2019 and projections for 2030 and 2045: results from the International Diabetes Federation Diabetes Atlas, 9th edition. *Diabetes Res Clin Pract*. 2019;157:107843. doi:10.1016/j.diabres.2019.107843
2. Shan JY, Zhang XX, Cheng Y, et al. Glucose metabolism-inspired catalytic patches for NIR-II phototherapy of diabetic wound infection. *Acta Biomater*. 2023;157:200–209. doi:10.1016/j.actbio.2022.12.001
3. Wang L, Hussain Z, Zheng PH, et al. A mace-like heterostructural enriched injectable hydrogel composite for on-demand promotion of diabetic wound healing. *J Mat Chem B*. 2023;11(10):2166–2183. doi:10.1039/D2TB02403A
4. Zhao X, Chang L, Hu Y, et al. Preparation of photocatalytic and antibacterial MOF nanozyme used for infected diabetic wound healing. *ACS Appl Mater Interfaces*. 2022;14(16):18194–18208. doi:10.1021/acsami.2c03001
5. Guan L, Ou X, Wang Z, et al. Electrical stimulation-based conductive hydrogel for immunoregulation, neuroregeneration and rapid angiogenesis in diabetic wound repair. *Sci China Mater*. 2023;66(3):1237–1248. doi:10.1007/s40843-022-2242-y
6. Wang S, Zheng H, Zhou L, et al. Nanoenzyme-reinforced injectable hydrogel for healing diabetic wounds infected with multidrug resistant bacteria. *Nano Lett*. 2020;20(7):5149–5158. doi:10.1021/acs.nanolett.0c01371
7. Lu BT, Ye HL, Shang SM, et al. Novel wound dressing with chitosan gold nanoparticles capped with a small molecule for effective treatment of multiantibiotic-resistant bacterial infections. *Nanotechnology*. 2018;29(42):425603. doi:10.1088/1361-6528/aad7a7
8. Zou Y, Xie R, Hu E, et al. Protein-reduced gold nanoparticles mixed with gentamicin sulfate and loaded into konjac/gelatin sponge heal wounds and kill drug-resistant bacteria. *Int J Biol Macromol*. 2020;148:921–931. doi:10.1016/j.ijbiomac.2020.01.190
9. Wang L, Yang J, Yang X, et al. Mercaptophenylboronic acid-activated gold nanoparticles as nanoantibiotics against multidrug-resistant bacteria. *ACS Appl Mater Interfaces*. 2020;12(46):51148–51159. doi:10.1021/acsami.0c12597
10. Pivodova V, Frankova J, Galandakova A, Ulrichova J. In vitro AuNPs' cytotoxicity and their effect on wound healing. *Nanobiomedicine*. 2015;2:7. doi:10.5772/61132
11. Zhao X, Tang H, Jiang X. Deploying gold nanomaterials in combating multi-drug-resistant bacteria. *Acs Nano*. 2022;16(7):10066–10087.
12. He X, Dai L, Ye L, et al. A vehicle-free antimicrobial polymer hybrid gold nanoparticle as synergistically therapeutic platforms for staphylococcus aureus infected wound healing. *Adv Sci*. 2022;9(14). doi:10.1002/advs.202105223
13. Ding JX, Gao BB, Chen ZH, Mei XF. An NIR-triggered au nanocage used for photo-thermo therapy of chronic wound in diabetic rats through bacterial membrane destruction and skin cell mitochondrial protection. *Front Pharmacol*. 2021;12. doi:10.3389/fphar.2021.779944
14. Zhao Y, Tian Y, Cui Y, Liu W, Ma W, Jiang X. Small molecule-capped gold nanoparticles as potent antibacterial agents that target gram-negative bacteria. *J Am Chem Soc*. 2010;132(35):12349–12356. doi:10.1021/ja1028843
15. Feng Y, Chen WW, Jia YX, et al. N-Heterocyclic molecule-capped gold nanoparticles as effective antibiotics against multi-drug resistant bacteria. *Nanoscale*. 2016;8(27):13223–13227. doi:10.1039/C6NR03317B
16. Ma Z, Garrido-Maestu A, Jeong KC. Application, mode of action, and in vivo activity of chitosan and its micro and nanoparticles as antimicrobial agents: a review. *Carbohydr Polym*. 2017;176:257–265. doi:10.1016/j.carbpol.2017.08.082
17. Lin X, Gong X, Ruan Q, Xu W, Zhang C, Zhao K. Antimicrobial application of chitosan derivatives and their nanocomposites. *Curr Med Chem*. 2023;30(15):1736–1755. doi:10.2174/0929867329666220803114729
18. Munoz-Nunez C, Cuervo-Rodriguez R, Echeverria C, Fernandez-Garcia M, Munoz-Bonilla A. Synthesis and characterization of thiazolium chitosan derivative with enhanced antimicrobial properties and its use as component of chitosan based films. *Carbohydr Polym*. 2023;302:120438. doi:10.1016/j.carbpol.2022.120438
19. Martins AF, Facchi SP, Follmann HDM, Pereira AGB, Rubira AF, Muniz EC. Antimicrobial activity of chitosan derivatives containing N-quaternized moieties in its backbone: a review. *Int J Mol Sci*. 2014;15(11):20800–20832. doi:10.3390/ijms151120800
20. Pan GX, Li FH, He SH, et al. Mussel- and barnacle cement proteins-inspired dual-bionic bioadhesive with repeatable wet-tissue adhesion, multimodal self-healing, and antibacterial capability for nonpressing hemostasis and promoted wound healing. *Adv Funct Mater*. 2022;32(25). doi:10.1002/adfm.202200908

21. Mihai MM, Dima MB, Dima B, Holban AM. Nanomaterials for wound healing and infection control. *Materials*. 2019;12(13):2176. doi:10.3390/ma12132176
22. Ou XL, Guan L, Guo WL, et al. Graphene oxide-based injectable conductive hydrogel dressing with immunomodulatory for chronic infected diabetic wounds. *Mater Des*. 2022;224:111284. doi:10.1016/j.matdes.2022.111284
23. Gong W, Wang R, Huang H, et al. Construction of double network hydrogels using agarose and gallic acid with antibacterial and anti-inflammatory properties for wound healing. *Int J Biol Macromol*. 2023;227:698–710. doi:10.1016/j.ijbiomac.2022.12.085
24. Li C, He X, Li Q, et al. A photothermal-response oxygen release platform based on a hydrogel for accelerating wound healing. *NPG Asia Materials*. 2023;15(1). doi:10.1038/s41427-022-00456-7
25. Chen SA, Chen HM, Yao YD, Hung CF, Tu CS, Liang YJ. Topical treatment with anti-oxidants and Au nanoparticles promote healing of diabetic wound through receptor for advance glycation end-products. *Eur J Pharm Sci*. 2012;47(5):875–883. doi:10.1016/j.ejps.2012.08.018
26. Saravanakumar K, Mariadoss AVA, Sathiyaseelan A, Wang MH. Synthesis and characterization of nano-chitosan capped gold nanoparticles with multifunctional bioactive properties. *Int J Biol Macromol*. 2020;165:747–757. doi:10.1016/j.ijbiomac.2020.09.177
27. Youssef AM, Abdel-Aziz MS, El-Sayed SM. Chitosan nanocomposite films based on Ag-NP and Au-NP biosynthesis by Bacillus Subtilis as packaging materials. *Int J Biol Macromol*. 2014;69:185–191. doi:10.1016/j.ijbiomac.2014.05.047
28. Zemlyakova ES, Tcibulnikova AV, Slezhkin VA, Zubin AY, Samusev IG, Bryukhanov VV. The infrared spectroscopy of chitosan films doped with silver and gold nanoparticles. *J Polymer Eng*. 2019;39(5):415–421. doi:10.1515/polyeng-2018-0356
29. Lu BT, Lu F, Ran LX, et al. Imidazole-molecule-capped chitosan-gold nanocomposites with enhanced antimicrobial activity for treating biofilm-related infections. *J Colloid Interface Sci*. 2018;531:269–281. doi:10.1016/j.jcis.2018.07.058
30. Ouyang Z, Bai S. Preparation and in-vitro biocompatibility of Gelatin/SA/HYA composite scaffold for tissue engineering. *Polymers Polymer Composites*. 2015;23(7):503–508. doi:10.1177/096739111502300709
31. Ying X, Yu C, Yang W, et al. The transformation of multifunctional bio-patch to hydrogel on skin wounds for efficient scarless wound healing. *Mater Today Bio*. 2024;24:100901. doi:10.1016/j.mtbio.2023.100901
32. Yang ZF, Huang RK, Zheng BN, et al. Highly stretchable, adhesive, biocompatible, and antibacterial hydrogel dressings for wound healing. *Adv Sci*. 2021;8(8). doi:10.1002/advs.202003627
33. Li J, Zhai Y-N, J-p X, et al. An injectable collagen peptide-based hydrogel with desirable antibacterial, self-healing and wound-healing properties based on multiple-dynamic crosslinking. *Int J Biol Macromol*. 2024;259(Pt 1):129006. doi:10.1016/j.ijbiomac.2023.129006
34. Li S, Li X, Xu Y, et al. Collagen fibril-like injectable hydrogels from self-assembled nanoparticles for promoting wound healing. *Bioact Mater*. 2024;32:149–163. doi:10.1016/j.bioactmat.2023.09.012
35. Liu R, Cai J, Qin N, et al. Nontoxic chemical crosslinked bacterial cellulose-heparin-gelatin composite hydrogel as antibacterial dressing. *J Mater Sci Technol*. 2024;178:29–38. doi:10.1016/j.jmst.2023.08.040
36. Oueslati MH, Ben Tahar L, Harrath AH. Catalytic, antioxidant and anticancer activities of gold nanoparticles synthesized by kaempferol glucoside from Lotus leguminosae. *Arab J Chem*. 2020;13(1):3112–3122. doi:10.1016/j.arabjc.2018.09.003
37. Volkova N, Yukhta M, Pavlovich O, Goltsev A. Application of cryopreserved fibroblast culture with au nanoparticles to treat burns. *Nanoscale Res Lett*. 2016;11. doi:10.1186/s11671-016-1242-y
38. Zhou X, Wang Z, Chan YK, et al. Infection micromilieu-activated nanocatalytic membrane for orchestrating rapid sterilization and stalled chronic wound regeneration. *Adv Funct Mater*. 2022;32(7):2109469.
39. Shi CY, Wang CY, Liu H, et al. Selection of appropriate wound dressing for various wounds. *Front Bioeng Biotechnol*. 2020;8. doi:10.3389/fbioe.2020.00182
40. Martin P, Nunan R. Cellular and molecular mechanisms of repair in acute and chronic wound healing. *Br J Dermatol*. 2015;173(2):370–378. doi:10.1111/bjd.13954
41. Wang Z, Ou XL, Guan L, et al. Pomegranate-inspired multifunctional nanocomposite wound dressing for intelligent self-monitoring and promoting diabetic wound healing. *Biosens Bioelectron*. 2023;235:115386. doi:10.1016/j.bios.2023.115386
42. Roy S, Santra S, Das A, et al. Staphylococcus aureus biofilm infection compromises wound healing by causing deficiencies in granulation tissue collagen. *Ann Surg*. 2020;271(6):1174–1185. doi:10.1097/SLA.0000000000003053
43. Gao WD, Jin WW, Li YN, et al. A highly bioactive bone extracellular matrix-biomimetic nanofibrous system with rapid angiogenesis promotes diabetic wound healing. *J Mat Chem B*. 2017;5(35):7285–7296. doi:10.1039/C7TB01484H
44. Zhu J, Zhou H, Gerhard EM, et al. Smart bioadhesives for wound healing and closure. *Bioact Mater*. 2023;19:360–375. doi:10.1016/j.bioactmat.2022.04.020
45. Zhou L, Liu F, You J. et al. A novel self-pumping janus dressing for promoting wound immunomodulation and diabetic wound healing. *Adv Healthcare Mater*;2023. e2303460. doi:10.1002/adhm.202303460
46. Zhang B, Lv Y, Yu C, et al. Au-Pt nanozyme-based multifunctional hydrogel dressing for diabetic wound healing. *Biomater Adv*. 2022;137:212869. doi:10.1016/j.bioadv.2022.212869